Spatial and temporal variability of groundwater recharge in a sandstone aquifer in a semi-arid region

Ferdinando Manna [1], Steven Murray [2], Daron Abbey [2], Paul Martin [2,3], John Cherry [1], Beth Parker [1]

[1] G[360] Institute for Groundwater Research, College of Engineering and Physical Sciences, University of Guelph, Guelph, Ontario, Canada

[2] Matrix Solutions Inc., Guelph, Ontario, Canada

[3] Aqua Insight Inc., Waterloo, Ontario, Canada.

Abstract

With the aim to understand the spatial and temporal variability of groundwater recharge, a high-resolution, spatially-distributed numerical model (MIKE SHE) representing surface water and groundwater was used to simulate responses to precipitation in a 2.16 km^2 upland catchment on fractured sandstone near Los Angeles, California. Exceptionally high temporal and spatial resolution was used for this catchment modeling: hourly climate data, a 20x20 meter grid in the horizontal plane and 240 numerical layers distributed vertically within the thick vadose zone and in the upper part of the groundwater zone. The finest-practical spatial and temporal resolution were selected to accommodate the large degree of surface and subsurface variability of catchment features. Physical property values for the different lithologies were assigned based on previous on-site investigations whereas the parameters controlling streamflow and evapotranspiration were derived from calibration to continuous streamflow at the outfall and to average hydraulic heads from 17 wells. Confidence in the calibrated model was enhanced by validation through, i) comparison of simulated average recharge to estimates based on the applications of the chloride mass-balance method to data from the groundwater and vadose zones within and beyond the catchment and, ii) comparison of the

water isotope signature (^{18}O and ^{2}H) in shallow groundwater to the variability of isotope signatures for precipitation events over an annual cycle and, iii) comparison of simulated recharge time series and observed fluctuation of water levels. The average simulated recharge across the catchment for the period 1995-2014 is 16 mm y^{-1} (4% of the average annual precipitation), which is consistent with previous estimates obtained by using the chloride mass balance method (4.2% of the average precipitation). However, one of the most unexpected results was that local recharge was simulated to vary from 0 to > 1000 mm y^{-1} due to episodic precipitation and overland runoff effects. This recharge occurs episodically with the major flux events at the bottom of the evapotranspiration zone, as simulated by MIKE SHE and confirmed by the isotope signatures, occurring only at the end of the rainy season. This is the first study that combines MIKE SHE simulations with the analysis of water isotopes in groundwater and rainfall to determine the timing of recharge in a sedimentary bedrock aquifer in a semi-arid region. The study advances the understanding of recharge and unsaturated flow processes and enhances our ability to predict the effects of surface and subsurface features on recharge rates. This is crucial in highly heterogeneous contaminated sites because different contaminant source areas have widely varying recharge and, hence, groundwater fluxes impacting their mobility.

Introduction

Assessment of groundwater recharge is fundamental to create strategies for management of water resources and to estimate volumetric groundwater flow through contaminated sites. Recharge rates represent an indication of upper limit of the volume of precipitation that may be accessible for sustainable use and can govern the volume of water available to transport contaminants. Its importance is greater in semi-arid regions where dominance of evapotranspiration limits water resources. In these regions, estimated recharge rates depend on the temporal and spatial resolution of the investigation and the uncertainties associated with recharge values are usually large

(Scanlon, 2000; Xie et al., 2018; Crosbie et al., 2018). In favorable circumstances, geochemical-based methods have proven to be especially useful for estimating recharge rates. In areas where the geologic and anthropogenic sources of chloride in the subsurface are negligible, the distribution of chloride in the vadose zone and groundwater has been used to calculate long-term site-wide (Wood and Sanford, 1995; Gebru and Tesfahunegn, 2018; Jebreen et al., 2018) and location-specific recharge values (Heilweil et al., 2006; Huang et al., 2018), to determine mechanisms of flow in the vadose zone (Sukhija et al., 2003; Li et al., 2017), and to evaluate the effects of environmental changes on recharge (Scanlon et al., 2007; Cartwright et al., 2007). Elevated tritium in precipitation derived from atmospheric releases during nuclear tests in the 1960's and transported into the subsurface has also been an invaluable tracer to determine modern recharge and mechanisms of flow in both vadose and groundwater zones (Cook and Böhlke, 2000; De Vries and Simmers, 2002). These geochemical and isotopic techniques are based on the interpretation of hydrologic process influences on the distribution of tracers in the subsurface but cannot show the dynamic, short-term temporal effects nor provide a continuous spatial representation of these processes at the catchment scale.

Numerical hydrologic models that integrate surface water and groundwater flows have been developed to simulate the spatial and temporal distribution of surface runoff, infiltration, evapotranspiration and groundwater recharge. However, the application of nearly all such simulation tools have been limited to humid regions (Wheater et al., 2007) with minimal application to semiarid regions. Scanlon et al. (2006), in their review on recharge in semiarid areas, reported only 7 papers providing a continuous spatial distribution of recharge, out of a total of 98 studies. However, these studies investigated large areas, from 1,039,647 km^2 (Flint and Flint, 2007) to 60 km^2 (Flint et al., 2001), using a relatively coarse spatial resolution (from 72,900 m^2 - Flint and Flint, 2007 to 900 m^2 - Flint et al., 2001). In the last decade, although modeling techniques have advanced to include combined surface water-groundwater simulations, recharge in semiarid areas

has been represented with a GIS approach (Hernández-Marín et al., 2018) often using remote sensing data (Wang et al., 2008; Coelho et al., 2017; Crosbie et al., 2015) or neglecting the surface water component and focusing on unsaturated zone (Levy et al., 2017; Turkeltaub et al., 2015).

Among the commercially available models, the physically based MIKE SHE represents the land-based hydrologic system, with an integration of the surface flows (i.e. precipitation, infiltration, evapotranspiration and runoff) and subsurface flows (i.e., percolation into the vadose zone and recharge across the water table) (Ma et al., 2016). However, the literature shows only two applications of MIKE SHE to assess recharge in semiarid areas. Liu et al. (2007) analyzed the recharge response associated with overland flow in an alluvial watershed (surface area: 91 km^2 - cell size: 2,500 m^2) in the Tarim Basin, China. Smerdon et al. (2009) distinguished and quantified the contributions of three sources to the total recharge for a valley bottom aquifer in the Okanagan Basin (Canada) (surface area: 130 km^2 - cell size: 10,000 m^2).

In this study encompassing a 20-year period (1995-2014), we used MIKE SHE to simulate the recharge and the other hydrologic processes in a small catchment (2.16 km^2) located on an exposed bedrock upland plateau (from 650 to 490 m asl) in the Simi Hills, near Los Angeles, California (Fig. 1). The area is semi-arid with potential evapotranspiration (CIMIS, 1999) exceeding the average annual precipitation (396 mm as the recorded average annual precipitation over the 1995 -2014 period). The bedrock consists of sandstone with interbeds of shale and siltstone, densely fractured with bedding parallel partings and vertical joints and faults (Cilona et al., 2015; Cilona et al., 2016; Link et al., 1984; MWH, 2016) (Fig. 2). The hydrogeology of the site has been investigated intensively over the past 20 years because of the chemical contamination (mainly Trichloroethene - TCE) in groundwater (Pierce et al., 2018a; Pierce et al., 2018b; Sterling et al., 2005; MWH, 2009; Cherry J.A., 2009) and construction and application of a 3-D flow model (FeFlow) has been an on-going effort supporting characterization and corrective measures (AquaResource and MWH, 2007). From the application at the site of the chloride mass balance (CMB), based on measurement of

chloride in atmospheric deposition, surface water and groundwater, Manna et al. (2016) estimated a long-term average recharge of 19 mm y^{-1}, corresponding to the 4.2 % of the average precipitation (455 mm for the period 1878-2014). More recently, Manna et al. (2017) analyzed porewater Cl concentration profiles from the vadose and groundwater zones at 11 locations across the site. This provided spatially variable, long-term recharge values ranging from 4 to 23 mm y^{-1} and indicated that, on average, 80% of the flow in the vadose zone occurs as intergranular flow in the rock matrix and 20% as fracture flow. These chloride-based methods lump together hydrologic processes providing long-term recharge estimates for only few locations across a large site. However, to inform the 3-D groundwater flow model and to simulate plume fluxes, information about the spatial and temporal distribution of recharge is needed.

In this study, we analyze the spatial and temporal variability of recharge in a catchment of the contaminated site not only to constrain recharge values but also to uncover hydrologic processes that cause the borehole-scale spatial variability observed in those previous studies (Manna et al., 2016; Manna et al., 2017). The catchment was chosen because it is representative of the varied surface and subsurface conditions found throughout the contaminated area and it is believed to be minimally impacted during the calibration period by the surface water controls measures in place. Given that the scope of the paper is to simulate the natural conditions, these initiatives are not considered in our modeling. To better represent the large range of surface and subsurface features and provide high-resolution representation of the spatial distribution of recharge, we used hourly climate data, sub-hourly time step and a fine grid of 400 m^2 cells for a total of 5,420 cells. In addition to the spatial variability, we also examined the seasonal dynamics of the hydrologic processes by tracking vadose zone water budgets for representative cells of the model. This analysis helped in understanding the transient conditions that determine the rates of the hydrologic processes throughout the year. The model was calibrated using measurements of runoff from instrumented outfall flows and quarterly observations of groundwater levels in 17 wells

distributed across the catchment for the simulated period. Unlike the previous applications of MIKE SHE in the literature, the simulation results were also validated through comparison with transient water levels from shallow wells, comparison with previous independent recharge estimates based on application of the Chloride Mass Balance (Manna et al., 2016; Manna et al., 2017) and through the analysis of water isotopes from rainfall and groundwater that indicated the timing of recharge. Finally, we proposed a conceptual model for various recharge conditions in the fractured sandstone aquifer based on the results of the MIKE SHE simulation along with findings of previous recharge studies for the site (Manna et al., 2016; Manna et al., 2017). In particular, the MIKE SHE simulations contributed to the conceptual model concerning the role of surface feature variability (e.g. topography and vegetation) on the hydrological processes whereas the Cl-based studies informed the flow mechanisms in the underlying portion of the system.

The site MIKE SHE model

The MIKE SHE model (Refsgaard, 1995) simulations were conducted at a sub-hourly time step using hourly meteorological data measured from 1995 through 2014 on site and from stations proximal to the study area. A portion of the rainfall is intercepted by the vegetation canopy, from which evaporation occurs. The remaining water reaches the surface, where it may infiltrate, evaporate or runoff downslope if depression storage is satisfied. Water infiltrating into the subsurface may be evapotranspired back to the atmosphere or percolate down to the water table to become groundwater recharge. Actual evaporation and transpiration were simulated based on the Kristensen and Jensen Evapotranspiration Model (Kristensen and Jensen, 1975), which considers potential evapotranspiration estimated using the FAO 56 Penman-Monteith method (Allen et al., 1998), available soil moisture and the crop characteristics (depth of the evapotranspiration zone, leaf area index and crop coefficient) in each grid cell (Table 1). When the rainfall exceeds the

148 infiltration capacity, water is ponded on the ground surface and is available for runoff. The
149 infiltration capacity in the model is dynamic and a function of the unsaturated hydraulic
150 conductivity (K_u) and the water content properties (i.e., saturation point, field capacity and
151 permanent wilting point) of the surficial media. To describe the relation between water content,
152 conductivity and matric potential, the Van Genuchten model is used (Van Genuchten, 1980).The
153 rate of runoff is simulated using a 2D diffusive wave approximation and is controlled by the
154 topographic slope, the surface roughness and detention storage. The latter is the volume of water
155 stored in surface depressions before runoff starts. The unsaturated zone flow is simulated as the
156 change in soil moisture, resulting from cyclical input (infiltration) and output (recharge and
157 evapotranspiration). It is modelled as a 1D column using the full Richards equations (Richards,
158 1931) with finite difference cells that have variable discretization from the top of the column
159 (ground surface) to the base of the column (the unsaturated/saturated zone interface). Given the
160 variable thickness of the vadose zone and the low water fluxes, the model was run several times to
161 set consistent initial conditions. Our analysis began when the simulation showed that the degree of
162 change in average recharge value from one run to the next was about 0.3% indicating near steady-
163 state conditions. Recharge was calculated anytime that infiltration water arrives at the water table.
164 Most precipitation events do not result in recharge because infiltration into the shallow subsurface
165 is intercepted and evapotranspired. The flow in the groundwater zone was represented using 3D
166 finite difference Darcy equation. A fixed head boundary applied along the lateral sides and the
167 bottom of the model domain (490 m asl) was used to simulate the flow to and from the deeper
168 groundwater system, not explicitly represented in the integrated model but which extends several
169 hundred meters (Fig. 3). These fixed heads are based on observed groundwater levels at the site
170 and simulations based on a detailed 3-D groundwater flow model system that includes the
171 catchment and a much larger domain beyond (AquaResource and MWH, 2007). The groundwater
172 contribution to streamflow is minimal and intermittent ($\sim$ 0.1 mm y^{-1} for the period of 1995-2014)

and only occurs at the farthest downstream location of the catchment where the groundwater table rises close to the ground surface.

Climate data

Hourly rainfall data were collected from two stations within the catchment boundaries: the Sage Ranch station, managed by Ventura County watershed (http://www.vcwatershed.net/hydrodata/php/getstation.php?siteid=272#top) and the Simi Hills-Rocketdyne Lab, managed by Boeing Inc. The annual precipitation ranges from 99 mm (2014) to 976 (1998), with an average value of 396 mm y^{-1}. The seasonal precipitation regime is Mediterranean, with 77% of the total precipitation occurring from December to March.

Daily maximum and minimum air temperature observations were obtained from two climate stations of the NOAA network: from 1995 to 1998 data were gathered from the Cheeseboro station (https://www.ncdc.noaa.gov/cdo-web/datasets/GHCND/stations/GHCND:USR0000CCHB/detail) and from 1998 to 2015 from the Van Nuys station (https://www.ncdc.noaa.gov/cdo-web/datasets/GSOM/stations/GHCND:USW00023130/detail), respectively 6 km SW and 18 km E of the study site. Temperatures were adjusted using a dry (10 $^{0}C\ km^{-1}$) and wet (5.5 $^{0}C\ km^{-1}$) adiabatic lapse rate based on the elevation change between the SSFL site and the collecting station. July, August and September are the warmest months with an average daily maximum temperature of 30.5, 31 and 30.4 ^{0}C, respectively whereas February and December are the coldest with an average daily maximum temperature of 17and 17.4 ^{0}C, respectively. Annual average temperature is 16.7^{0}C.

Surface and subsurface parameters

The MIKE SHE model was developed employing a 20 by 20 m finite-difference horizontal-plane grid to represent the surface physical features, a fine vertical discretization of the vadose zone with 240 numerical layers ranging from 0.1 to 1 m thickness and 2 groundwater zone layers, with thickness

variable from 5 to 185 m, to represent vertical variability at, and just below, the position of the water table (Fig. 3). This resolution was selected as a compromise between representation of spatial variability at a more detailed scale and reasonable computational time. Maps of topography, vegetation, surficial geology and land use were used to assign surface parameters (Fig. 1, Fig. 2 and Fig. 4). High resolution topographic data (2 feet interval elevation contours) were obtained based on an aerial survey of the site in 2010. These topography data were used to define the ground surface elevations (Fig. 1).

The surface and subsurface hydrogeologic units include alluvium, fractured weathered and unweathered bedrock comprised of sandstone, siltstone and shale beds of varying thickness, grain size and cementation (Fig. 2 and Fig. 3). The physical properties of these units, derived from previous on-site investigations (Allegre et al., 2016; Quinn et al., 2015; Quinn et al., 2016) and adjusted by calibration, are summarized in Table 2. In particular, our model uses three separate sets of Van Genuchten parameters to represent the pressure saturation-hydraulic conductivity relationships. The parameters used reflect our understanding that the rock matrix transmits the largest volume of recharge (80%), while recharge through the fractures is minimal (20%) (Manna et al., 2017). Therefore, the relationships used are biased towards the matrix response. These values were further calibrated using the groundwater level responses and the streamflow. Further rock core samples indicate a high moisture content (~80%) (Cherry et al., 2009) indicating that K_u is often close to K_s and the hydraulic conductivity-saturation curve reflects this understanding.

Four land use classes were identified and delineated based on aerial imagery and local land cover datasets (Davis et al., 1998): developed areas (roads, building, parking lots); chaparral (chamise, scrub oak), coastal scrub (Black sage) and exposed bedrock (areas without vegetation) (Fig. 4). The first category represents only 5% of the study catchment whereas the two vegetation classes (chaparral and coastal sage scrub) cover 83% of the area. The remaining 12% is represented by bedrock outcrop. This latter category was subdivided into two classes: non-massive bedrock and

massive bedrock based on physical appearance. Massive bedrock areas were identified based on rock masses that have resisted erosion over the decades and are presumed to be poorly-fractured and/or well cemented such that local infiltration through these rock units is very low. These cell assignments were identified using topography and imagery analysis. First, we used the minimum downslope elevation change approach to identify topographic ridges; this algorithm calculates the minimum elevation drop to a downslope neighbor. In a second stage, we isolate from the land use map the exposed bedrock areas. Vegetation, indeed, generally does not grow on well cemented rock. Finally, massive bedrock areas were assigned cells with downslope elevation change greater than 1.25 meters in areas without vegetation.

Values of Leaf Area Index, depth of the root zone, surface roughness and Manning's number were assigned to each land use class-specific parameters, based on the calibration process, with final values similar to those available in the literature (Canadell et al., 1996; Scurlock et al., 2001; Chin et al., 2000) (Table 1). To calculate the actual evapotranspiration, a crop coefficient varying monthly between 0.53 and 1.02 has been used. This estimate are based on i) reference crop evapotranspiration rates (RET) for Zone 9 of the Reference Evapotranspiration Zones map of the California Irrigation Management Information System, that corresponds with the area the site is within (ITRC, 2003), ii) a 'Pasture and Misc. grasses' land class chosen as representative of the site and iii) a reduction of 8% to account for bare spots in vegetation and reduced vigor (ITRC, 2003).

Unsaturated zone water budgets

To assess the temporal variability of infiltration, evapotranspiration, change in storage and recharge, we extracted the simulated unsaturated zone water budgets for two locations representing the span of variability of the catchment. The two locations were selected based on surface geology (Fig. 2) and land use category (Fig. 4): UZ1 represents an area of outcropping bedrock without vegetation and UZ2 represents a cell with alluvium and vegetation cover. The

246 average infiltration value over the simulated period at the two locations (UZ-1: 87 mm y^{-1}; UZ-2:
247 395 mm y^{-1}) matches the average infiltration value for all the cells of the catchments with same land
248 use and surface geology. For these cells, we extracted the weekly time series of infiltration,
249 evapotranspiration, storage variations and flux at the bottom of the ET zone (i.e., drainage). The
250 latter indicates the volume of water that infiltrates into the vadose zone and will eventually become
251 recharge upon reaching the water table. The analysis of the seasonal variability of these fluxes
252 provided insights about their transient nature and about the effect of the surface variability on the
253 hydrologic processes in the unsaturated zone.

254 *Approach for model calibration*

255 In the model calibration procedure, the simulation results were compared to observed processes
256 and, to obtain acceptable matches, 10 parameters were available to adjust: surface roughness,
257 detention storage, imperviousness, rooting depth, leaf area index (LAI), crop coefficient,
258 unsaturated hydraulic conductivity and water content parameters of alluvium and weathered
259 bedrock. These were tested against an objective function of streamflow and groundwater level
260 measurements. An objective function is a measure of overall model fit of simulated to observed
261 values of groundwater levels and streamflow.

262 For the streamflow calibration, we compared the surface runoff generated by MIKE SHE to the data
263 collected at the catchment outfall between 2009 to 2011. This time interval had minimal
264 occurrence of substantial anthropogenic activities and was representative of natural hydrologic
265 conditions, as reported also by Manna et al. (2016).

266 For the calibration to groundwater levels, quarterly manually measured water level data were used.
267 Excluded from the calibration data were: i) wells with screened interval below the bottom of the
268 model domain (490 m a.s.l.), and ii) wells where the water table is strongly influenced by
269 subsurface complexity not represented in the saturated zone portion of the MIKE SHE model. After

these exclusions, water level data from 17 wells being used with water depths ranging from 25 to 137 meters bgs (Fig. 1, 2 and 4). The number of measurements in the time series at each well varies from 1 (RD-130) to 139 (WS-09B) measurements. In the calibration procedure, average values were used for comparison with average simulated values.

The calibration process proceeded in an iterative manner. After each calibration run, the two calibration targets were examined with a variety of metrics. For the streamflow, we analyzed mean error for simulated and observed average annual flow; mean error, root mean squared error, correlation and Nash Sutcliffe Efficiency for the simulated and observed average monthly and daily flows. An additional qualitative measure of the correlation between precipitation and streamflow event was provided by the analysis of the graphical of plots of observed and simulated daily streamflow hydrographs.

For the groundwater levels, the metrics were mean error, mean absolute error, root mean squared error and normalized root mean squared error for the simulated and observed average water levels. In addition, residual plots of simulated and observed water levels provided a quantitative and qualitative assessment of the residual error present at the observation well throughout the domain. Spatial patterns of groundwater level residual were compared against other spatial data (e.g. hydraulic conductivity, boundary conditions, land uses, surface geology) to evaluate potential correlations and adjustments that could improve the calibration.

Following an assessment of these calibration targets, the ten model parameters were adjusted for better calibration metrics. In instances where the results were not consistent with the site conceptualization, consideration was given as to whether an alternative conceptualization would explain the results predicted by the model. Testing of alternative conceptualizations through manual simulations was chosen over the alternative method of optimization of a single conceptualization using software such as PEST (Doherty, 2004) given the uncertainty in how to

294 parameterize models in these semi-arid environments. Given the structural changes
295 (representation of the unsaturated flow, representation of impervious areas) that were made to the
296 model during the several simulations, it was not possible to carry out an exhaustive optimization or
297 sensitivity analysis. However, through the calibration process we gained semi-quantitative
298 information about the model sensitivity to each parameter which is presented in the results section.

299

300 *Approach for model validation*

301 To obtain confidence about the reasonableness of the results, simulation results from the calibrated
302 model were tested by a validation procedure, which included comparison to previous independent
303 recharge estimates based on chloride, and timing of recharge from isotopic data (^{18}O – ^{2}H) and from
304 analysis of observed fluctuations of water level hydrographs, not used in the calibration. The
305 premise of the validation is that the calibrated model must provide results consistent with the
306 validation information, that are entirely independent of the parameter assignments made in the
307 calibration.

308 Manna et al. (2016) estimated an average long-term recharge of 19 mm y^{-1} for the same catchment
309 using the chloride mass balance (CMB) method, based on the average Cl concentration measured in
310 the atmospheric deposition, comprised of rainfall and dry fallout (2.6 mg L^{-1}), surface water at the
311 catchment outfall (4 mg L^{-1}) and groundwater (52.5 mg L^{-1}). Since chloride concentration in
312 groundwater is proportional to the concentrating effect of water loss due to evapotranspiration, it
313 can be used as a proxy to determine the range of variability in recharge. Chloride concentration in
314 shallow groundwater monitoring wells ranges across the area from 17 to 162 mg/L corresponding
315 to recharge values of 43 and 5 mm y^{-1}, respectively. Manna et al (2017) also provided insights
316 regarding spatial variability of recharge within the catchment based on analysis of Cl profiles in
317 porewater from the vadose zone and groundwater which indicate a range of recharge from 4 to 21

318 mm y^{-1} corresponding to <1 – 4.7% of the average annual precipitation for 4 locations located
319 within the catchment area. Although the recharge values obtained from the CMB method integrate
320 hydrologic processes occurring over longer time, from decades to millennia, they represent a
321 reasonable assessment of long-term, site-wide and location-specific average values and are
322 valuable for validation purposes.

323 Samples of rainfall and groundwater were analyzed for water isotopes (^{18}O – ^{2}H) . These water
324 isotopes are commonly used to assess evaporative processes and to determine sources and origins
325 of different groundwaters. Typically, the water isotope values vary seasonally over the annual cycle,
326 so that the groundwater composition reflects the season with most of the recharge. In this study,
327 we compared the isotopic signature of groundwater to that of precipitation for an entire
328 hydrological year to determine whether the timing of recharge indicated by the model is consistent
329 with the isotopic signature for the same period of the year. The available isotope data for rainfall
330 were determined for the period October 1994 to June 1995 collected at two rain gauge stations
331 (B/886 and RMDF), 5 km from the studied watershed and analyzed in the same year by an
332 automated gas-source mass spectrometer at the University of California Berkeley. The groundwater
333 samples were collected from monitoring wells in the studied catchment in two rounds of sampling:
334 the first in 2003-2004 and the second in 2013 (Fig. 1).

335 Furthermore, to test the ability of the model to simulate unsaturated zone flow processes and to
336 reproduce the transient recharge conditions, we compared the simulated time series of recharge,
337 obtained from MIKE SHE, with quarterly water level measurements at five locations not used in the
338 calibration process. The depth to groundwater at these wells ranges between 2 and 60 m with
339 seasonal fluctuations due to the recharge events. The recharge time series is obtained, extracting
340 the average, catchment-wide, monthly recharge values.

341

Simulation results

Model calibration and sensitivity

Streamflow measured at the outfall occurs in response to rainfall; however, some precipitation events are followed by very low or no measurable flow (Fig. 5). This is evident for precipitation events from April to June 2009, October and November 2010 and May and June 2011. In all these cases, the surface runoff, generated by the precipitation events, infiltrates into the subsurface without reaching the surface outfall (Fig. 5). These hydrologic dynamics are well simulated by MIKE SHE. The comparison between the observed and the simulated hydrographs shows a good correlation for the calibration period (R^2=0.97; average difference 4.7%). The average simulated flow is 48 mm y^{-1}, about 14.5% of the average precipitation for the 2009-2011 period (331 mm) and is almost coincident with the measured flow (46.2 mm y^{-1}) (Fig. 5). This value reflects the precipitation conditions of the 2009-2011 period and is lower than the average runoff over the entire simulated interval (110 mm y^{-1}, 28% of the annual precipitation). Monthly and daily Nash Sutcliffe Efficiency (NSE) values of 0.94 and 0.87 were achieved respectively, indicating good fit to observed flows (NSE=1 corresponds to a perfect match).

In addition to the surface water leaving the catchment, the model was also calibrated to the observed average groundwater head data (Fig. 6). A good match was obtained for the 17 locations, with almost all values falling within the 10 m confidence interval bands, with a correlation coefficient of 0.96 and a mean absolute error of 4.5 m (Fig. 6). This good correlation provides confidence about the spatial distribution of model parameters.

Of the 10 adjusted parameters, unsaturated hydraulic conductivity and water content parameters of alluvium and weathered bedrock had the strongest effect on the calibration and are, therefore, well constrained by the measured streamflow and groundwater levels. These geologic features represent the upper layers of the model domain and variations in their physical and hydraulic

properties control the rate of infiltration, evapotranspiration, drainage and, therefore, recharge. A third parameter important in the calibration was the detention storage. This is because a substantial amount of water from precipitation, especially at the beginning of the rainy season, infiltrates without generating runoff events at the outfall (Fig. 5). This volume of water is controlled not only by the properties of unsaturated zone (Table 2) but also by the value of detention storage assigned to each land use class (Table 1). Conversely, alterations in rooting depth, LAI and crop coefficient only resulted in small changes in streamflow. This is because significant runoff events tend to occur during brief high-intensity precipitation events with a magnitude that far exceeds the relative amount of evapotranspiration, which might occur during these events. For the same reason, though, these factors had a relatively greater effect on the volume of water available for drainage and subsequent recharge.

Spatial variability

To study the spatial variability of the water budget components, average annual maps of infiltration (Fig. 7a), evapotranspiration (Fig. 7b) and recharge (Fig. 7c) for the period 1995 – 2014 were created.

Average infiltration for the catchment is 254 mm y^{-1}, corresponding to 64% of the total precipitation but single cell values span over three orders of magnitude from 9 to > 1000 mm y^{-1} (Fig. 7a). Low infiltration values are found in developed/paved (average 51 mm y^{-1}) and massive-bedrock (average 14 mm y^{-1}) cells. Due to the low infiltration capacity, more runoff is generated in these cells and, thus, infiltration is higher in nearby cells that receive the surface water. Where these neighboring cells are covered by alluvium at the surface, infiltration is even higher. On average, cells with alluvium at the surface have an infiltration value of 332 mm y^{-1}, 25% more than those where bedrock outcrops. Higher infiltration is also displayed in depressed areas such as

those along the main drainages and where closed topographic depressions occur. These cells collect most of the surface runoff creating conditions for focused infiltration and recharge.

Only a small portion of water that enters the subsurface reaches the water table because the majority is lost due to evapotranspiration (Fig. 7b). The average evapotranspiration estimated using MIKE SHE is 265 mm y^{-1}, a value slightly higher than the average infiltration. This excess of ET over infiltration is attributed to canopy interception and evaporation of temporarily ponded surface water. When removing these two water-loss processes, the average evapotranspiration is 237 mm y^{-1}, which corresponds to 60% of the annual precipitation and to 94% of the total infiltration. Transpiration is the main process of ET contributing to about 70% of the total ET. This result is expected considering the considerable depth of the roots (up to 5 meters for Chaparral) and the fact that vegetation covers 83% of the catchment area. Single cell values of ET span over three orders of magnitude, from 50 to >1000 mm y^{-1}. Since the actual evapotranspiration depends strongly on the availability of subsurface water, the spatial variability mimics the infiltration pattern and the two factors are strongly correlated (R^2=0.84). Therefore, low ET is associated with developed (asphalt, buildings) and massive bedrock areas and high ET values are found along the main surface drainages where infiltration is high and locally available for evapotranspiration. The presence of alluvium at the surface increases the ET values on average by 25%; for example, average ET in cells with chaparral and alluvium is 400 mm y^{-1} whereas where chaparral is rooted in weathered bedrock is ~300 mm y^{-1}.

A map of the spatial distribution of the average annual recharge is shown in Fig. 7c. The average recharge value for the catchment is 16 mm y^{-1} equal to 4.1 % of the precipitation and 6.5 % of the infiltration. The range of variability of recharge is over three orders of magnitude and spatially variable depending on topography, surface geology and land use. It is noteworthy that 79% of the catchment has recharge less than 10 mm y^{-1} and 90% less than 30 mm y^{-1}, which indicates that the largest volumes of recharge are focused in small portions of the site. The recharge map (Fig. 7c)

shows the influence of the surface parameters on recharge estimates. Recharge is high along the main drainage because of the contribution of surface water flowing from the surrounding slopes and enhanced infiltration where the topographic slope decreases abruptly. Relatively higher recharge values are also observed in areas with alluvium at the surface because the infiltration and retention capacities are higher and, therefore, water can seep from the overburden into the bedrock once the evapotranspiration demand and driving forces are met. Recharge is also higher in cells without vegetation cover, compared to other cells with equivalent topographic slope and surficial geology, because the evapotranspiration in these areas is lower.

Temporal variability

The seasonal variability of the hydrologic processes was examined analyzing unsaturated water budgets at two locations with different land use and surficial geology (UZ-1 and UZ-2 in Fig.1) Among the 20 years, we show the monthly average daily values from 2005 to 2007. This time span features a wet year (2005 – 978 mm), a dry year (2007 – 149 mm) and one year with average precipitation (2006 - 331 mm) and therefore is reasonably representative of the simulated period.

For areas with bedrock outcrop not covered by vegetation (UZ-1 in Fig. 1), the infiltration ranges from 0 to 2.5 mm d^{-1} (Fig. 8). The infiltration pattern shows null or minimal values during the summer and positive events during the wet season. Water that enters the subsurface between April and January replenishes the water content in the ET zone and becomes available for evaporation but not for drainage. Evaporation is null during the summer because of the lack of precipitation and because all the water stored in the first 20 cm of bedrock has been taken up by evaporation in the previous months. Downward flux at the bottom of the ET zone (i.e. drainage) only happens episodically when the water content in the ET zone is above the field capacity, at the end of the wet

438 season (i.e., March and April) or occasionally after exceptionally high-intensity precipitation events
439 (i.e., January 2005).

440 For areas with alluvium at surface (UZ-2 in Fig. 1) the infiltration has the same pattern but a
441 different order of magnitude (from 0 to 30 mm d^{-1}) due to the higher infiltration capacity of the
442 alluvium (Fig. 8). Here, the available water capacity of the ET zone is greater because of the
443 different physical properties (e.g. larger porosity) of the soil and the greater depth of the ET zone.
444 Therefore, almost all the infiltration water is taken up by the evapotranspiration. Unlike areas
445 without vegetation, evapotranspiration is not directly related to precipitation events and occurs
446 more continuously throughout the year. This is because alluvium stores a greater volume of water
447 in the ET zone that is nearly completely consumed by ET. A drainage flux is observed only during
448 high-intensity precipitation events that create near-saturation conditions such that water cannot be
449 held by tension in the shallow unsaturated zone and downward flow is initiated.

450 For both cases, drainage is not steady throughout the year but occurs episodically, controlled by
451 antecedent soil water content in the ET zone and by the intensity of precipitation. During drier-
452 than-average years, such as 2007, drainage occurs in areas without vegetation, whereas no
453 drainage is observed in cells with vegetation cover. After crossing the bottom of the ET zone, water
454 arrives at the water table with a time lag depending on the magnitude of the flux and on the
455 physical properties and the thickness of the vadose zone.

456 *Model validation*

457 The ability of the model to simulate transient hydrologic conditions was investigated through the
458 comparison between well hydrographs at five locations and the temporal variability of recharge
459 (Fig. 9). The spatially-average recharge rates obtained from MIKE SHE (monthly time-step) range
460 from 0.95 mm (November 2014) to 9.1 mm (March 2005). The latter is the response to the
461 extraordinary rainy season that occurred between December 2004 and March 2005 (903 mm)

462 whereas the first is due to dry conditions of the recent drought in California. The range of depth to
463 groundwater from 1995 to 2014 at the five locations considered is 2.8 – 14.4 m at RD-09, 17.8 – 30
464 m at RD-35A, 16.2 – 28.7 at RD-73, 37.7 – 50.8 m at RD-36B and 33.1 – 60.1 at WS-09B. The shape
465 of these hydrographs depends on surface (surface geology, topographic slope, land use) and
466 subsurface (mechanisms of flow in the vadose zone) conditions. For our validation purpose, it is
467 noteworthy that, at all the locations, the hydrographs show a good match with the recharge time
468 series such that the peaks in recharge coincide with water table rises. The greatest rises overlap the
469 two highest recharge periods (1998 and 2005), whereas a constant declining trend is observed
470 from 2011 to 2014 in response to drier conditions (Fig. 9). The good correlation suggests that, at
471 this scale, the equivalent porous media approach used is reasonable to simulate average responses
472 in groundwater because, although the bedrock has many interconnected fractures, it is only a minor
473 contributor to recharge.

474 The average recharge value for the catchment from the simulation is 16 mm y^{-1} and is consistent
475 with previous recharge estimates obtained for the site using the CMB method (19 mm y^{-1} – 4.2% of
476 the average precipitation, Manna et al., 2016; 16 mm y^{-1} – 3.5% of the average precipitation, Manna
477 et al., 2017). The frequency distribution of recharge values from the MIKE SHE simulation (92% of
478 the domain has average recharge lower than 40 mm y^{-1}) also corresponds well to the range of
479 variability based on chloride (from 0 to 43 mm y^{-1}) reported by Manna et al. (2016) and Manna et
480 al. (2017).

481 For additional information on recharge processes, we analyzed water isotopes obtained from
482 rainfall and groundwater samples (Fig. 10). The samples show a substantial isotopic range from
483 one precipitation event to another over the one-year collection period. ^{18}O varies between -2.8 and
484 -12.1‰ for B/886 and -2.8 and -11.7‰ for RDMF and ^{2}H varying between -11 and -89‰ for B/886
485 and -12 and -85‰ for RDMF (Table 3). This large range of values is probably due to the two

different trajectories of the precipitation events in southern California, one originating in the Pacific and one over the Gulf of Mexico, as found by Friedman et al. (1992). The volume weighted mean values for the two stations are -8.2 and -54.2‰ for B/886 and -8.2 and -56.2‰ for RDMF and are consistent with global-scale maps of water isotopes for precipitation in southern California (Bowen and Revenaugh, 2003).

Unlike rainfall, groundwater samples fall within a narrower range: from -6.5 to -7.5‰ for ^{18}O and from -40.2 and to -52.2‰ for ^{2}H. All the samples are aligned along the local meteoric water line (Fig. 10) indicating little if any evaporation from standing water on surface. This lack of concentration effect on the isotopes is apparently in contrast to the chloride data. Manna et al. (2016) found that Cl concentrations in groundwater are, on average, 20 times greater those from atmospheric deposition because of the strong influence of evapotranspiration. The common explanation for the lack of evaporation effects on the water isotopes in groundwater is that the transpiration is the main evapotranspiration process (Clark, 2015;Cook and Böhlke, 2000). Although transpiration through the vegetation causes a concentration effect on Cl, it does not cause fractionation of the water isotopes and therefore the groundwater samples are not enriched (Clark, 2015; Cook and Böhlke, 2000).

The lack of evaporative water isotope signature associated with high groundwater Cl concentration can also be explained by recharging water that crosses the ET zone mobilizing precipitated salts but without any evaporation. This hypothesis supports the results of the MIKE SHE simulations, which show that throughout the year there are only episodic fluxes at the bottom of the ET zone (Fig. 9). A relevant observation that corroborates this hypothesis is that the isotopic composition of groundwater is similar to that found in rainfall samples collected at the end of the wet season (March and June) or, on occasion, with high-intensity precipitation events (January - 203 mm) (Table 3). This similarity can be attributed to the preponderance of recharge occurring at these

510 times and thereby resulting in the groundwater values being different from the weighted mean
511 precipitation by 1.2‰ ^{18}O and 3‰ ^{2}H.

512 This proposed model of episodic flow through the unsaturated ET zone is also corroborated by the
513 evidence presented by Manna et al., (2017) that, on average, 20% of the flow in the vadose zone
514 occurs as fast flow through the interconnected fractured network.

515

516 **Discussion and conceptual model for recharge**

517 To summarize the findings of this study, and its relationship to the literature and to the previous
518 recharge studies at the site (Manna et al., 2016; Manna et al., 2017), we propose the following
519 process-based conceptual model for site recharge (Fig. 11).

520 The average recharge value is 16 mm y^{-1} which is consistent with previous estimates at the site, and
521 with those obtained for other sandstone aquifers in semi-arid areas in the United States (4% -
522 Heilweil et al., 2006) and other studies in semi-arid regions around the world (0.2 – 35 mm y^{-1} equal
523 to 0 – 5% of the average precipitation, Scanlon et al., 2006). Recharge varies greatly across the
524 catchment as a function of topography, surface geology, and land use. High recharge occurs where
525 most runoff water seeps into the subsurface, creating conditions for focused recharge. This
526 condition happens where closed depressions occur and where sloped topography abruptly
527 transitions to flat along the main surface drainages (Fig. 11a). In most areas, alluvium covers the
528 fractured porous bedrock, thus enhancing infiltration and temporary storage of infiltrated water.
529 Generally, in semiarid regions, high recharge values along a valley, at the edge of the slope referred
530 to as Mountain Front Recharge (MFR) (Wilson and Guan, 2004). However, our catchment is located
531 on the top of a ridge standing 300 m above the surrounding valleys (Manna et al., 2016) and, thus,
532 our case study represents groundwater recharge on the mountain block rather than MFR.
533 Nonetheless, it is interesting that the processes observed in our small catchment are similar to

those described for aquifer-scale recharge studies (Aishlin and McNamara, 2011; Carling et al., 2012; Manning and Solomon, 2003; Bresciani et al., 2018) and defined as MFR.

Infiltration from April to December (dry season) contributes to replenish the water content in the ET zone and remains available for evapotranspiration (Fig. 11b). Conversely, during the wet season, infiltration crosses the bottom of the ET zone (i.e. drainage) and migrates deeper through the vadose zone. This happens when the soil is above the field capacity (FC), which is more frequent at the end of the wet season in March or April and/or during high-intensity precipitation events, (Fig. 11c). This recharging water quickly crosses the ET zone, as shown by the ET zone water budgets extracted from MIKE SHE (Fig. 9), and by the lack of evaporative signature in isotope composition (Fig. 10).

The occurrence of this fast/preferential flow out of the ET zone is also corroborated by the analysis of vertical chloride porewater concentration profiles in the unsaturated zone (Manna et al., 2017). The Cl concentration is high in the ET zone (up to 10,000 mg L^{-1}) and considerably lower in deeper vadose and groundwater zones (average 49 mg L^{-1}). The higher Cl concentrations in the shallow subsurface is the effect of strong evapotranspiration that takes up water but not chloride, whereas the lower concentration below is due to fast/preferential flow of water that escapes the concentrating effect of water loss in the shallower zone. Case studies showing similar results for water that crosses the ET zone preferentially in time and space to become potentially recharge have been also reported in literature (Kurtzman et al., 2016), also referred to as selective recharge (Gat and Tzur, 1967; Florea, 2013; Krabbenhoft et al., 1990) . The occurrence of these fluxes has been also analyzed in function of precipitation characteristics and antecedent water content with rainfall intensity being the main factor (Allocca et al., 2015; Crosbie et al., 2012; Nasta et al., 2018; Taylor et al., 2013).

Upon reaching the deeper vadose zone, water is redistributed between intergranular matrix flow and fracture flow due to wettability and saturation concepts. The fractures and the matrix pores drain the water from the ET zone. Active flow through the fractures is possible under conditions such as ponding or intense precipitation, when a continuous slug of water lets i) the advective front move ahead into the fracture (1 in Fig. 11c); ii) the matrix water flow into the fractures (2 in Fig. 11c). Otherwise, water is drawn from the fractures into the unsaturated matrix blocks (3 in Fig. 11c) and contributes to the slow vertical intergranular matrix flow (4 in Fig. 11c). According to Manna et al. (2017), the first two mechanisms are much less frequent and contribute, on average, to only 20% of the total recharge. It is most likely that conditions for flow in the fractures occur episodically in areas of the site with high infiltration (topographic low and alluvium at the surface) where temporary perched systems are observed.

Conclusions

For the upland bedrock catchment, the surface water-groundwater numerical model (MIKE SHE), using a fine numerical grid (20 ×20 m) with calibration to streamflow and groundwater levels, simulated the spatial and temporal variability of recharge across a 2.16 km^2 catchment in southern California, USA. This is the first study that combined MIKE SHE simulations supported by analysis of water isotopes and chloride mass balance to assess recharge in a sedimentary bedrock aquifer in a semi-arid region. The calibrated simulations, indeed, were judged to be reliable and strongly reflective of the natural system, based on the validation comparisons to mean recharge obtained independently from the chloride mass balance method (Manna et al., 2016; Manna et al., 2017) and to the timing of major recharge events indicated by water isotopes and water level fluctuations. The simulations showed that major flux events at the bottom of the evapotranspiration zone, that result in recharge tens of meters below the surface, occur episodically mostly at the end of the rainy

581 season and that recharge varies across the catchment between 0 and 1000 mm y^{-1}. The fine
582 numerical grid in the horizontal plane allowed meaningful examination of recharge spatial
583 variability. A substantially coarser grid would obscure influences of key surface features on the
584 hydrologic processes.

585 The results obtained from the catchment-scale simulations are being used to specify rules for
586 recharge to be assigned to the upper boundary condition of a 3-D numerical EPM groundwater flow
587 model (FeFlow), covering the studied catchment and a much large area beyond (52 km^2). The
588 modeled groundwater domain has many contaminant plumes and recharge is key to determine the
589 fluxes available to transport contaminants.

590 The aim of the MIKE SHE model is to represent the natural hydrologic conditions, after site
591 industrial operations ceased more than a decade ago. During historical operations from 1950's
592 through mid-2000's, use of imported and pumped groundwater likely caused increases to
593 infiltration and recharge locally in some areas. These conditions are beyond the scope of this paper
594 but worth further consideration in a follow-on study as it relates to when contaminant releases
595 occurred and may provide insights regarding how contaminant migration rates may have been
596 influenced. Future modeling efforts will also evaluate the effect on recharge of the surface water
597 control systems currently in place on the site. These storm water management measures aim to
598 limit the volume of water leaving the catchment and, therefore, will likely influence the natural
599 rates of the other hydrologic processes.

600

601 **Acknowledgements**

602 Funding for this work was provided by an NSERC Industrial Research Chair (n. IRCPJ 363783) to
603 Professor Beth Parker in partnership with the Boeing Company. Field work was supported by

the site owner, their consultants (MWH Inc., now Stantec), and University of Guelph colleagues, especially Amanda Pierce from the G^{360} Institute for Groundwater Research, who collected and analyzed isotope samples.

References

Aishlin, P., and McNamara, J. P.: Bedrock infiltration and mountain block recharge accounting using chloride mass balance, Hydrological Processes, 25, 1934-1948, 2011.

Allegre, V., Brodsky, E. E., Xue, L., Nale, S. M., Parker, B. L., and Cherry, J. A.: Using earth-tide induced water pressure changes to measure in situ permeability: A comparison with long-term pumping tests, Water Resources Research, 52, 3113-3126, 10.1002/2015wr017346, 2016.

Allen, R. G., Pereira, L. S., Raes, D., and Smith, M.: Crop evapotranspiration-Guidelines for computing crop water requirements-FAO Irrigation and drainage paper 56, Fao, Rome, 300, D05109, 1998.

Allocca, V., De Vita, P., Manna, F., and Nimmo, J. R.: Groundwater recharge assessment at local and episodic scale in a soil mantled perched karst aquifer in southern Italy, Journal of Hydrology, 529, 843-853, 10.1016/j.jhydrol.2015.08.032, 2015.

AquaResource, and MWH: Three-Dimensional Groundwater Flow Model Report. Santa Susana Field Laboratory., 2007.

Bowen, G. J., and Revenaugh, J.: Interpolating the isotopic composition of modern meteoric precipitation, Water Resources Research, 39, 2003.

624 Bresciani, E., Cranswick, R. H., Banks, E. W., Batlle-Aguilar, J., Cook, P. G., and Batelaan, O.: Using
625 hydraulic head, chloride and electrical conductivity data to distinguish between mountain-front and
626 mountain-block recharge to basin aquifers, Hydrology & Earth System Sciences, 22, 2018.

627 Canadell, J., Jackson, R. B., Ehleringer, J. R., Mooney, H. A., Sala, O. E., and Schulze, E. D.: Maximum
628 rooting depth of vegetation types at the global scale, Oecologia, 108, 583-595,
629 10.1007/bf00329030, 1996.

630 Carling, G. T., Mayo, A. L., Tingey, D., and Bruthans, J.: Mechanisms, timing, and rates of arid region
631 mountain front recharge, Journal of hydrology, 428, 15-31, 2012.

632 Cartwright, I., Weaver, T. R., Stone, D., and Reid, M.: Constraining modern and historical recharge
633 from bore hydrographs, H-3, C-14 and chloride concentrations: Applications to dual-porosity
634 aquifers in dryland salinity areas, Murray Basin, Australia, Journal of Hydrology, 332, 69-92,
635 10.1016/j.jhydrol.2006.06.034, 2007.

636 Cherry J.A., P. B. L., McWhorter D.: Site conceptual model for the migration and fate of contaminants
637 in groundwater at the Santa Susana Field Laboratory, Simi Valley, California., 2009.

638 Cherry, J. A., McWorther, D. B., and Parker, B. L.: Site conceptual model for the migration and fate of
639 contaminants in groundwater at the Santa Susana Field Laboratory, Simi, California (draft), vols 1–
640 4, Association with the University of Guelph, Toronto, ON; MWH, Walnut Creek, CA, 2009.

641 Chin, D. A., Mazumdar, A., and Roy, P. K.: Water-resources engineering, Prentice Hall Englewood
642 Cliffs, 2000.

643 Cilona, A., Aydin, A., and Johnson, N.: Permeability of a fault zone crosscutting a sequence of
644 sandstones and shales and its influence on hydraulic head distribution in the Chatsworth
645 Formation, California, USA, Hydrogeology Journal, 23, 405-419, 10.1007/s10040-014-1206-1,
646 2015.

647 Cilona, A., Aydin, A., Likerman, J., Parker, B., and Cherry, J.: Structural and statistical characterization
648 of joints and multi-scale faults in an alternating sandstone and shale turbidite sequence at the Santa
649 Susana Field Laboratory: Implications for their effects on groundwater flow and contaminant
650 transport, Journal of Structural Geology, 85, 95-114, 10.1016/j.jsg.2016.02.003, 2016.

651 CIMIS: Reference Evapotranspiration. Department of Land Arid and Water Resources, University of
652 California, Davis and Water Efficiency Office, California Department of Water Resources, California
653 Irrigation Management Unit., 1999.

654 Clark, I.: Groundwater geochemistry and isotopes, CRC press, 2015.

655 Coelho, V. H. R., Montenegro, S., Almeida, C. N., Silva, B. B., Oliveira, L. M., Gusmão, A. C. V., Freitas, E.
656 S., and Montenegro, A. A.: Alluvial groundwater recharge estimation in semi-arid environment using
657 remotely sensed data, Journal of Hydrology, 548, 1-15, 2017.

658 Cook, P. G., and Böhlke, J.-K.: Determining timescales for groundwater flow and solute transport, in:
659 Environmental tracers in subsurface hydrology, Springer, 1-30, 2000.

660 Crosbie, R. S., McCallum, J. L., Walker, G. R., and Chiew, F. H.: Episodic recharge and climate change
661 in the Murray-Darling Basin, Australia, Hydrogeology Journal, 20, 245-261, 2012.

662 Crosbie, R. S., Davies, P., Harrington, N., and Lamontagne, S.: Ground truthing groundwater-recharge
663 estimates derived from remotely sensed evapotranspiration: a case in South Australia,
664 Hydrogeology Journal, 23, 335-350, 10.1007/s10040-014-1200-7, 2015.

665 Crosbie, R. S., Peeters, L. J., Herron, N., McVicar, T. R., and Herr, A.: Estimating groundwater recharge
666 and its associated uncertainty: Use of regression kriging and the chloride mass balance method,
667 Journal of Hydrology, 561, 1063-1080, 2018.

668 Davis, F., Stoms, D., Hollander, A., Thomas, K., Stine, P., Odion, D., Borchert, M., Thorne, J., Gray, M.,
669 and Walker, R.: The California gap analysis project–final report. University of California, Santa
670 Barbara, CA, 1998.

671 De Vries, J. J., and Simmers, I.: Groundwater recharge: an overview of processes and challenges,
672 Hydrogeology Journal, 10, 5-17, 2002.

673 Doherty, J.: PEST model-independent parameter estimation user manual, Watermark Numerical
674 Computing, Brisbane, Australia, 3338, 3349, 2004.

675 Flint, A. L., Flint, L. E., Bodvarsson, G. S., Kwicklis, E. M., and Fabryka-Martin, J.: Evolution of the
676 conceptual model of unsaturated zone hydrology at Yucca Mountain, Nevada, Journal of Hydrology,
677 247, 1-30, 2001.

678 Flint, L. E., and Flint, A. L.: Regional analysis of ground-water recharge, Ground-water recharge in
679 the arid and semiarid southwestern United States, 29-59, 2007.

680 Florea, L. J.: Selective recharge and isotopic composition of shallow groundwater within temperate,
681 epigenic carbonate aquifers, Journal of hydrology, 489, 201-213, 2013.

682 Friedman, I., Smith, G. I., Gleason, J. D., Warden, A., and Harris, J. M.: Stable isotope composition of
683 waters in southeastern California 1. Modern precipitation, Journal of Geophysical Research:
684 Atmospheres, 97, 5795-5812, 1992.

685 Gat, J., and Tzur, Y.: Modification of the isotopic composition of rainwater by processes which occur
686 before groundwater recharge, Isotopes in hydrology. Proceedings of a symposium, 1967,

687 Gebru, T. A., and Tesfahunegn, G. B.: Chloride mass balance for estimation of groundwater recharge
688 in a semi-arid catchment of northern Ethiopia, Hydrogeology Journal, 1-16, 2018.

689 Heilweil, V. M., Solomon, D. K., and Gardner, P. M.: Borehole environmental tracers for evaluating
690 net infiltration and recharge through desert bedrock, Vadose Zone Journal, 5, 98-120, 2006.

691 Hernández-Marín, M., Guerrero-Martínez, L., Zermeño-Villalobos, A., Rodríguez-González, L.,
692 Burbey, T. J., Pacheco-Martínez, J., Martínez-Martínez, S. I., and González-Cervantes, N.: Spatial and
693 temporal variation of natural recharge in the semi-arid valley of Aguascalientes, Mexico,
694 Hydrogeology Journal, 26, 2811-2826, 2018.

695 Huang, Y., Chang, Q., and Li, Z.: Land use change impacts on the amount and quality of recharge
696 water in the loess tablelands of China, Science of the Total Environment, 628, 443-452, 2018.

697 ITRC: California Crop and Soil Evapotranspiration, ITRC Report No. R 03-001. 2003.

698 Jebreen, H., Wohnlich, S., Wisotzky, F., Banning, A., Niedermayr, A., and Ghanem, M.: Recharge
699 estimation in semi-arid karst catchments: Central West Bank, Palestine, Grundwasser, 23, 91-101,
700 2018.

701 Krabbenhoft, D. P., Bowser, C. J., Anderson, M. P., and Valley, J. W.: Estimating groundwater
702 exchange with lakes: 1. The stable isotope mass balance method, Water Resources Research, 26,
703 2445-2453, 1990.

704 Kristensen, K., and Jensen, S.: A model for estimating actual evapotranspiration from potential
705 evapotranspiration, Hydrology Research, 6, 170-188, 1975.

706 Kurtzman, D., Baram, S., and Dahan, O.: Soil–aquifer phenomena affecting groundwater under
707 vertisols: a review, Hydrology and Earth System Sciences, 20, 1-12, 2016.

708 Levy, Y., Shapira, R. H., Chefetz, B., and Kurtzman, D.: Modeling nitrate from land surface to wells'
709 perforations under agricultural land: success, failure, and future scenarios in a Mediterranean case
710 study, Hydrology & Earth System Sciences, 21, 2017.

711 Li, Z., Chen, X., Liu, W., and Si, B.: Determination of groundwater recharge mechanism in the deep
712 loessial unsaturated zone by environmental tracers, Science of the Total Environment, 586, 827-
713 835, 2017.

714 Link, M. H., Squires, R. L., and Colburn, I. P.: Slope and deep-sea fan facies and paleogeography of
715 Upper Cretaceous Chatsworth Formation, Simi Hills, California, AAPG Bulletin, 68, 850-873, 1984.

716 Liu, H.-L., Chen, X., Bao, A.-M., and Wang, L.: Investigation of groundwater response to overland flow
717 and topography using a coupled MIKE SHE/MIKE 11 modeling system for an arid watershed,
718 Journal of Hydrology, 347, 448-459, 2007.

719 Ma, L., He, C., Bian, H., and Sheng, L.: MIKE SHE modeling of ecohydrological processes: Merits,
720 applications, and challenges, Ecological Engineering, 96, 137-149, 2016.

721 Manna, F., Cherry, J. A., McWhorter, D. B., and Parker, B. L.: Groundwater recharge assessment in an
722 upland sandstone aquifer of southern California, Journal of Hydrology, 541, 787-799,
723 10.1016/j.jhydrol.2016.07.039, 2016.

724 Manna, F., Walton, K. M., Cherry, J. A., and Parker, B. L.: Mechanisms of recharge in a fractured
725 porous rock aquifer in a semi-arid region, Journal of Hydrology, 555, 869-880,
726 10.1016/J.Jhydrol.2017.10.060, 2017.

727 Manning, A. H., and Solomon, D. K.: Using noble gases to investigate mountain-front recharge,
728 Journal of Hydrology, 275, 194-207, 2003.

729 MWH: Draft-site wide groundwater remedial investigation report Santa Susana Field Laboratory,
730 Ventura County, California. Prepared for The Boeing Company, NASA and U.S. DOE by MWH Global
731 Inc., Walnut Creek, CA., 2009.

732 MWH: Hydrogeological Characterization of Faults. Santa Susana Field Laboratory, Ventura County,
733 Ca. Prepared for The Boeing Company by Dr. Nicholas M. Johnson, MWH Americas Inc., 2121 N.
734 California Blvd., Suite 600, Walnut Creek, CA 94596., 2016.

735 Nasta, P., Adane, Z., Lock, N., Houston, A., and Gates, J. B.: Links between episodic groundwater
736 recharge rates and rainfall events classified according to stratiform-convective storm scoring: A
737 plot-scale study in eastern Nebraska, Agricultural and Forest Meteorology, 259, 154-161, 2018.

738 Pierce, A. A., Chapman, S. W., Zimmerman, L. K., Hurley, J. C., Aravena, R., Cherry, J. A., and Parker, B.
739 L.: DFN-M field characterization of sandstone for a process-based site conceptual model and
740 numerical simulations of TCE transport with degradation, Journal of contaminant hydrology, 212,
741 96-114, 2018a.

742 Pierce, A. A., Parker, B. L., Ingleton, R., and Cherry, J. A.: Novel Well Completions in Small Diameter
743 Coreholes Created Using Portable Rock Drills, Groundwater Monitoring & Remediation, 38, 42-55,
744 2018b.

745 Quinn, P., Cherry, J. A., and Parker, B. L.: Combined use of straddle packer testing and FLUTe
746 profiling for hydraulic testing in fractured rock boreholes, Journal of Hydrology, 524, 439-454,
747 2015.

748 Quinn, P. M., Cherry, J. A., and Parker, B. L.: Depth-discrete specific storage in fractured sedimentary
749 rock using steady-state and transient single-hole hydraulic tests, Journal of Hydrology, 542, 756-
750 771, 2016.

751 Refsgaard, C.: Mike she, Computer models of catchment hydrology, 809-846, 1995.

752 Richards, L. A.: Capillary conduction of liquids through porous mediums, physics, 1, 318-333, 1931.

753 Scanlon, B. R.: Uncertainties in estimating water fluxes and residence times using environmental
754 tracers in an arid unsaturated zone, Water Resources Research, 36, 395-409, 2000.

755 Scanlon, B. R., Keese, K. E., Flint, A. L., Flint, L. E., Gaye, C. B., Edmunds, W. M., and Simmers, I.: Global
756 synthesis of groundwater recharge in semiarid and arid regions, Hydrological Processes: An
757 International Journal, 20, 3335-3370, 2006.

758 Scanlon, B. R., Reedy, R. C., and Tachovsky, J. A.: Semiarid unsaturated zone chloride profiles:
759 Archives of past land use change impacts on water resources in the southern High Plains, United
760 States, Water Resources Research, 43, 2007.

761 Scurlock, J., Asner, G., and Gower, S.: Worldwide historical estimates of leaf area index, 1932–2000,
762 ORNL/TM-2001/268, 34, 2001.

763 Smerdon, B., Allen, D., Grasby, S., and Berg, M.: An approach for predicting groundwater recharge in
764 mountainous watersheds, Journal of Hydrology, 365, 156-172, 2009.

765 Sterling, S., Parker, B., Cherry, J., Williams, J., Lane Jr, J., and Haeni, F.: Vertical cross contamination of
766 trichloroethylene in a borehole in fractured sandstone, Groundwater, 43, 557-573, 2005.

767 Sukhija, B., Reddy, D., Nagabhushanam, P., and Hussain, S.: Recharge processes: piston flow vs
768 preferential flow in semi-arid aquifers of India, Hydrogeology Journal, 11, 387-395, 2003.

769 Taylor, R. G., Todd, M. C., Kongola, L., Maurice, L., Nahozya, E., Sanga, H., and MacDonald, A. M.:
770 Evidence of the dependence of groundwater resources on extreme rainfall in East Africa, Nature
771 Climate Change, 3, 374, 2013.

772 Turkeltaub, T., Kurtzman, D., Russak, E., and Dahan, O.: Impact of switching crop type on water and
773 solute fluxes in deep vadose zone, Water Resources Research, 51, 9828-9842, 2015.

774 Van Genuchten, M. T.: A closed-form equation for predicting the hydraulic conductivity of
775 unsaturated soils 1, Soil science society of America journal, 44, 892-898, 1980.

776 Wang, H., Kgotlhang, L., and Kinzelbach, W.: Using remote sensing data to model groundwater
777 recharge potential in Kanye region, Botswana, 2008.

778 Wheater, H., Sorooshian, S., and Sharma, K. D.: Hydrological modelling in arid and semi-arid areas,
779 Cambridge University Press, 2007.

780 Wilson, J. L., and Guan, H.: Mountain-block hydrology and mountain-front recharge, Groundwater
781 recharge in a desert environment: The Southwestern United States, 9, 2004.

782 Wood, W. W., and Sanford, W. E.: Chemical and isotopic methods for quantifying ground-water
783 recharge in a regional, semiarid environment, Groundwater, 33, 458-468, 1995.

784 Xie, Y., Cook, P. G., Simmons, C. T., Partington, D., Crosbie, R., and Batelaan, O.: Uncertainty of
785 groundwater recharge estimated from a water and energy balance model, Journal of Hydrology,
786 561, 1081-1093, 2018.

Table 1 Land use class-specific parameters to model runoff and evapotranspiration.

Land Use Class	Surface roughness (Manning's n)	Detention storage (mm)	Leaf Area Index	Depth of the evapotranspiration zone (m)
Developed*	0.04	1	-	0.2
Coastal Scrub	0.2	7.5	1.8 - 3	1.8 - 3
Chaparral	0.2	7.5	2.8 - 4.5	3.1 - 5
Exposed Bedrock/ Massive bedrock*	0.05	3	-	0.2

Table 2 Physical properties of the different hydrogeologic units.

						Van Genuchten parameters		
Hydrogeologic unit	**Lithology**	**K_s (m s^{-1})**	**Saturation (θ_s)**	**Field capacity (θ_{fc})**	**Residual Water content (θ_r)**	**α**	**n**	**l**
Alluvium		1×10^{-6}	0.4	0.25	0.05	0.021	1.61	0.5
Weathered bedrock		2×10^{-7}	0.2	0.11	0.01	0.033	1.49	0.5
Unweathered bedrock	Shale/Siltstone	4.1×10^{-10} to 2.3×10^{-7}	0.13	0.1	0.025	0.01	1.23	0.5
Unweathered bedrock	Sandstone	1×10^{-10} to 1×10^{-5}	0.13	0.09	0.01	0.01	2	0.5

Unweathered bedrock	Fault zone	1×10^{-9} to 1×10^{-6}	0.13	0.1	0.025	0.01	2	0.5

796

797

798

799 *Table 3 Stable isotope composition of rainfall.*

Date	B/886 Rain Gauge			RMDF Rain Gauge			Average		
	$\delta^{18}O$	$\delta^{2}H$	Rainfall (mm)	$\delta^{18}O$	$\delta^{2}H$	Rainfall (mm)	$\delta^{18}O$	$\delta^{2}H$	Rainfall (mm)
4/10/1994	-4	-19	3				-4.0	-19.0	3
25/11/1994	-5.2	-18	6	-5.1	-16	6	-5.2	-17.0	6
13/12/1994	-5.4	-23	9	-5.4	-25	9	-5.4	-24.0	9
24/12/1994	-10.3	-77	18	-10.1	-69	18	-10.2	-73.0	18
4/1/1995	-10.3	-75	94	-9.9	-69	121	-10.1	-72.0	108
11/1/1995	-6	-33	205	-7.4	-45	202	-6.7	-39.0	203
13/01/1995	-4.4	-19	20	-4.2	-20	18	-4.3	-19.5	19
16/01/1995	-2.8	-11	12	-2.8	-12	10	-2.8	-11.5	11
26/01/1995	-12.1	-89	152	-11.7	-85	150	-11.9	-87.2	151
7/3/1995	-6.8	-43	119	-6.4	-40	109	-6.6	-41.5	114
13/3/1995	-7.5	-44	NA	-7.8	-45	NA	-7.7	-44.5	NA
24/3/1995	-5.8	-22	NA	-5.5	-19	NA	-5.7	-20.5	NA
18/5/1995				-6.4	-42	34	-6.4	-42.0	34
22/6/1995	-8.6	-62	14	-8.6	-57	14	-8.6	-59.5	14
Volume weighted mean and total rainfall	-8.2	-54.2	650	-8.2	-56.2	691	-8.3	-55.2	689

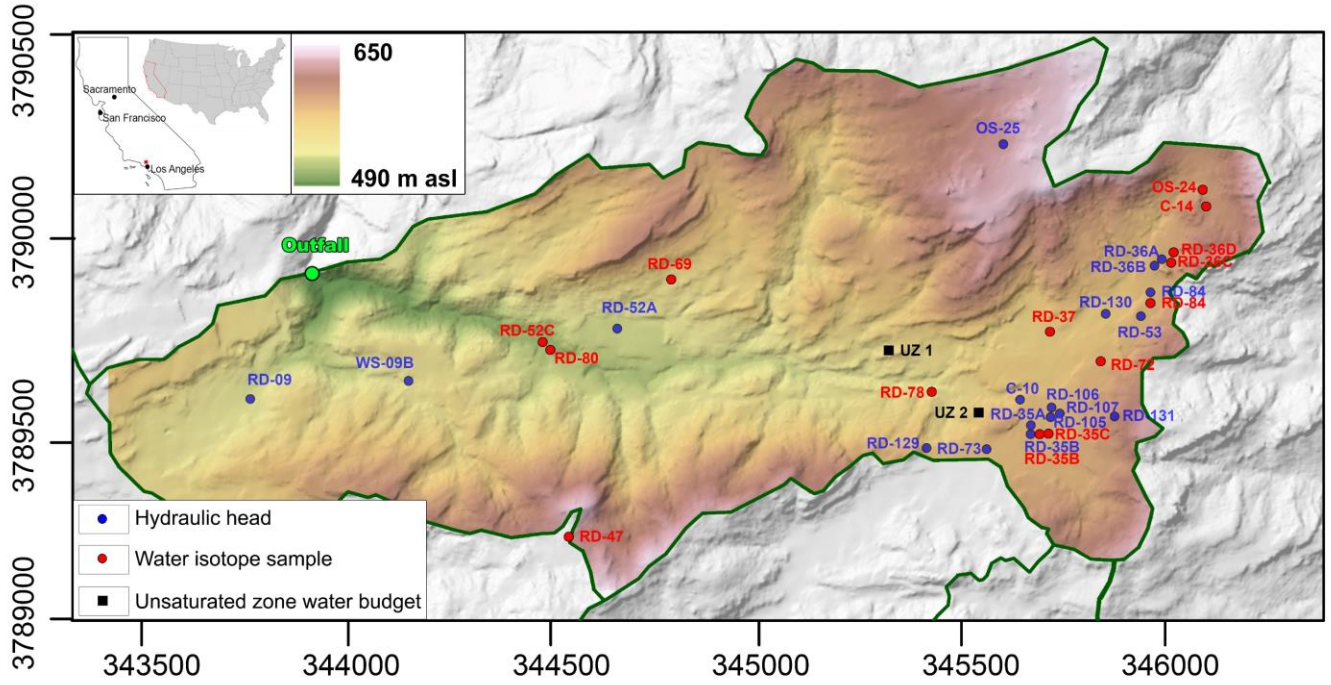

Figure 1 Topographic map of the study area and location of the wells used for calibration (blue), water isotopes sampling (red). In black the two cells where unsaturated zone water budgets were analyzed.

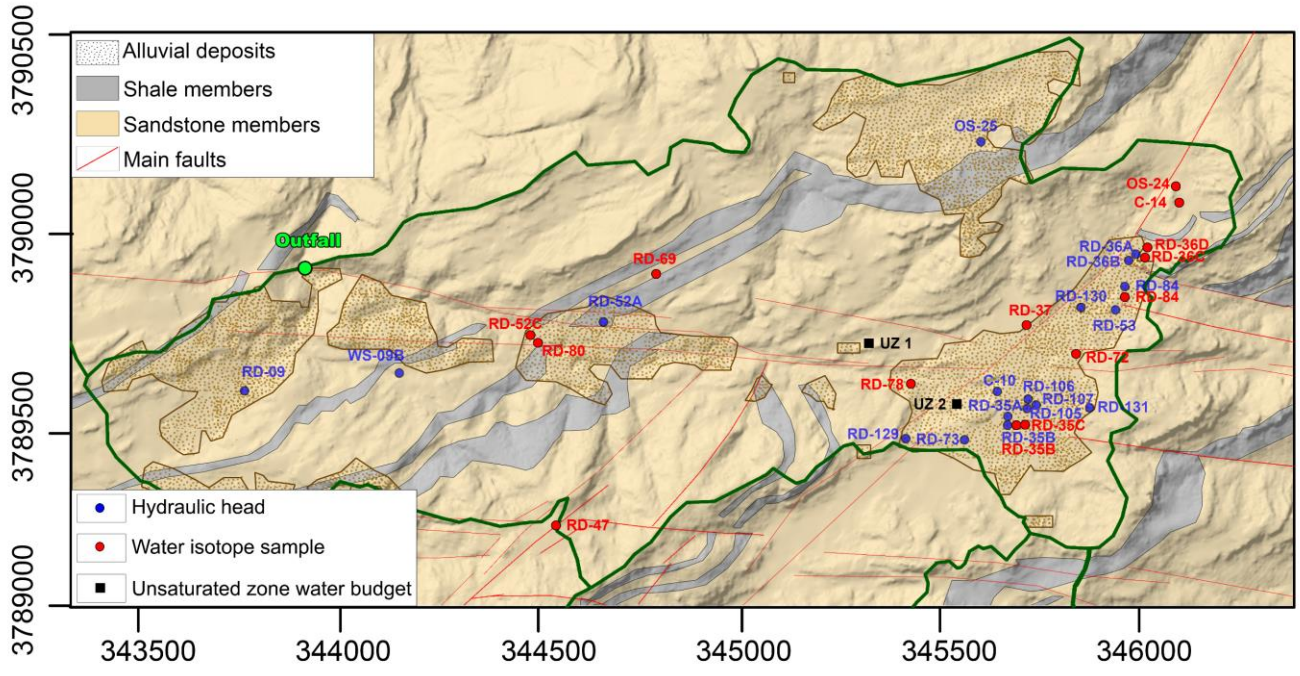

Figure 2 Geologic map of the study area and location of the wells used for calibration (blue), water isotopes sampling (red). In black the two cells where unsaturated zone water budgets were analyzed.

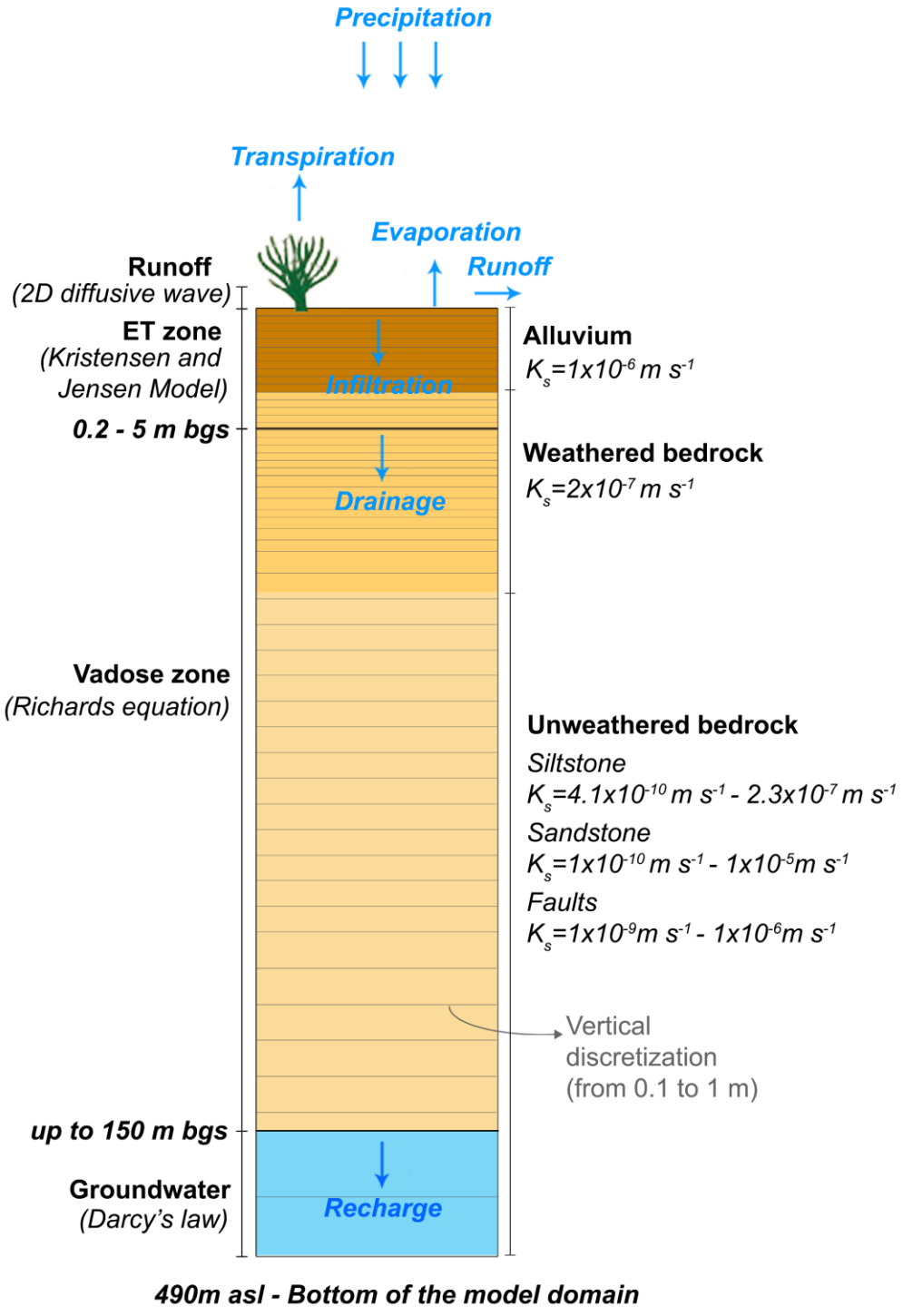

807

808 *Figure 3 Description of the vertical MIKE SHE model domain*

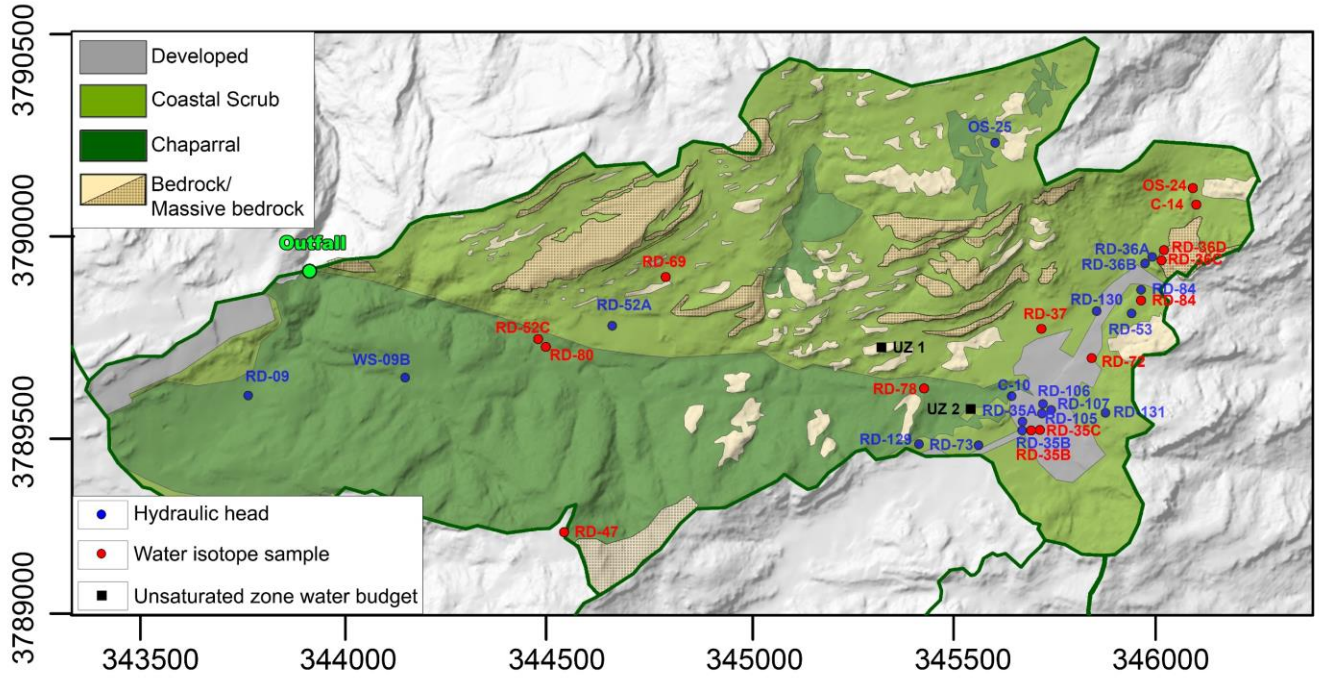

809

810 *Figure 4 Land use map and location of the wells used for calibration (blue), water isotopes sampling (red). In black the two*
811 *cells where unsaturated zone water budgets were analyzed.*

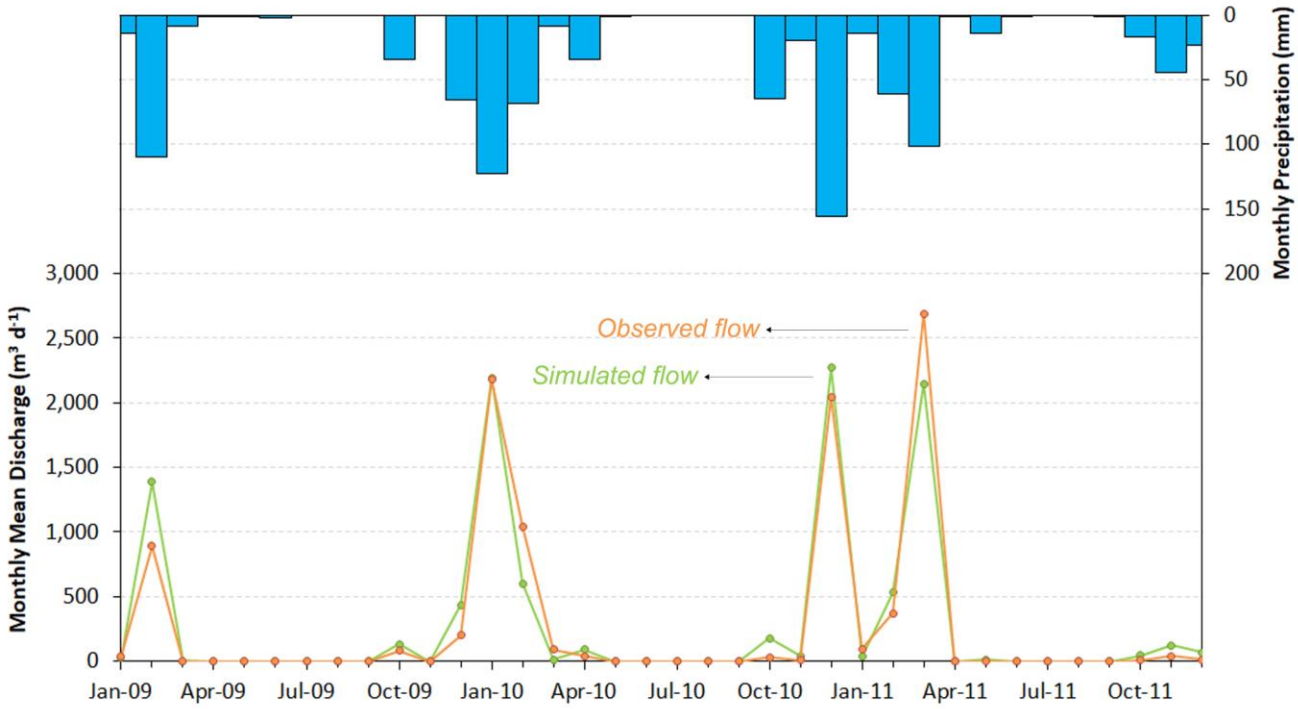

812

813 *Figure 5 Monthly precipitation values and comparison between simulated (green) and observed (red) runoff flow at the*
814 *outfall of the catchment from January 2009 to December 2011.*

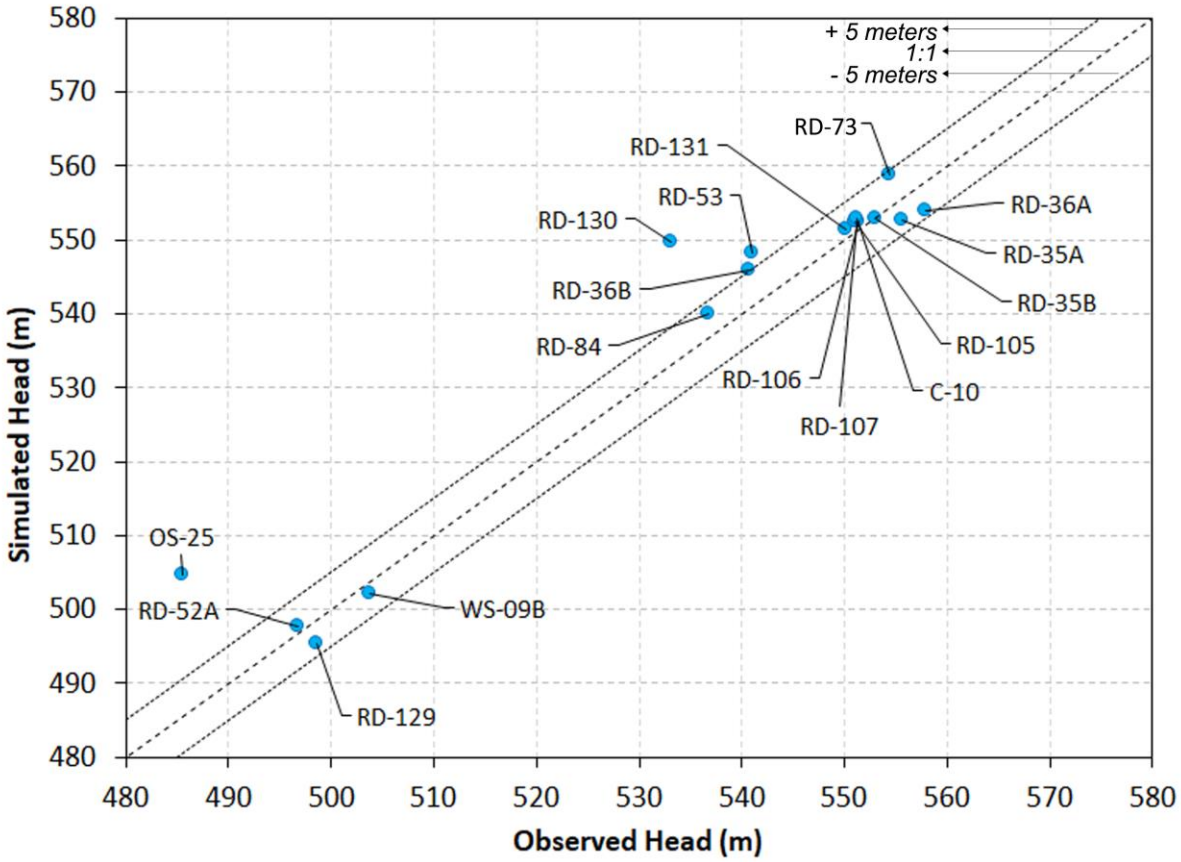

Figure 6 Comparison between simulated and observed groundwater head data for the 17 wells.

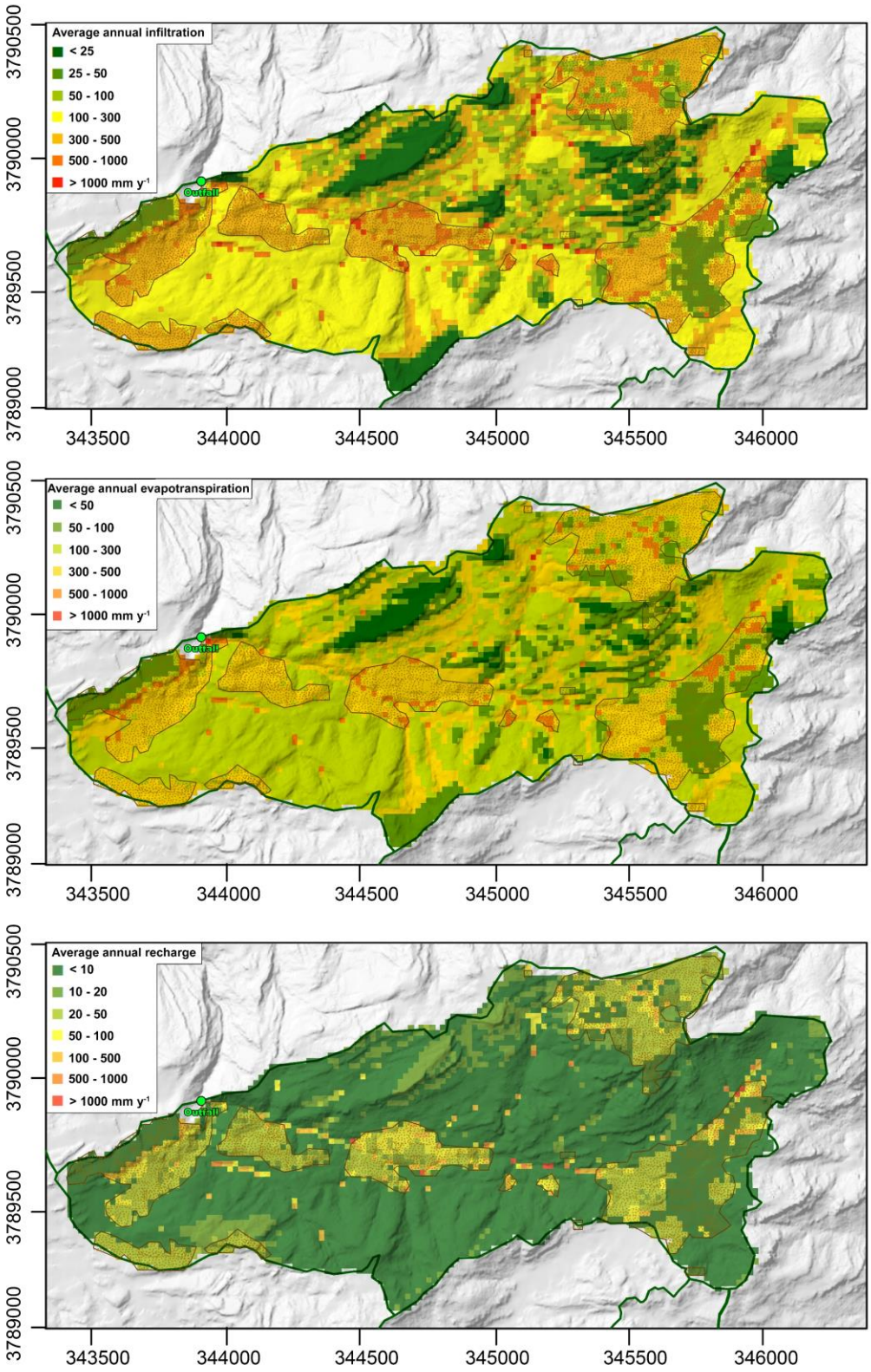

Figure 7. Distribution of average annual infiltration (a), evapotranspiration (b) and recharge (c). Dashed polygons represent areas with alluvium at the surface.

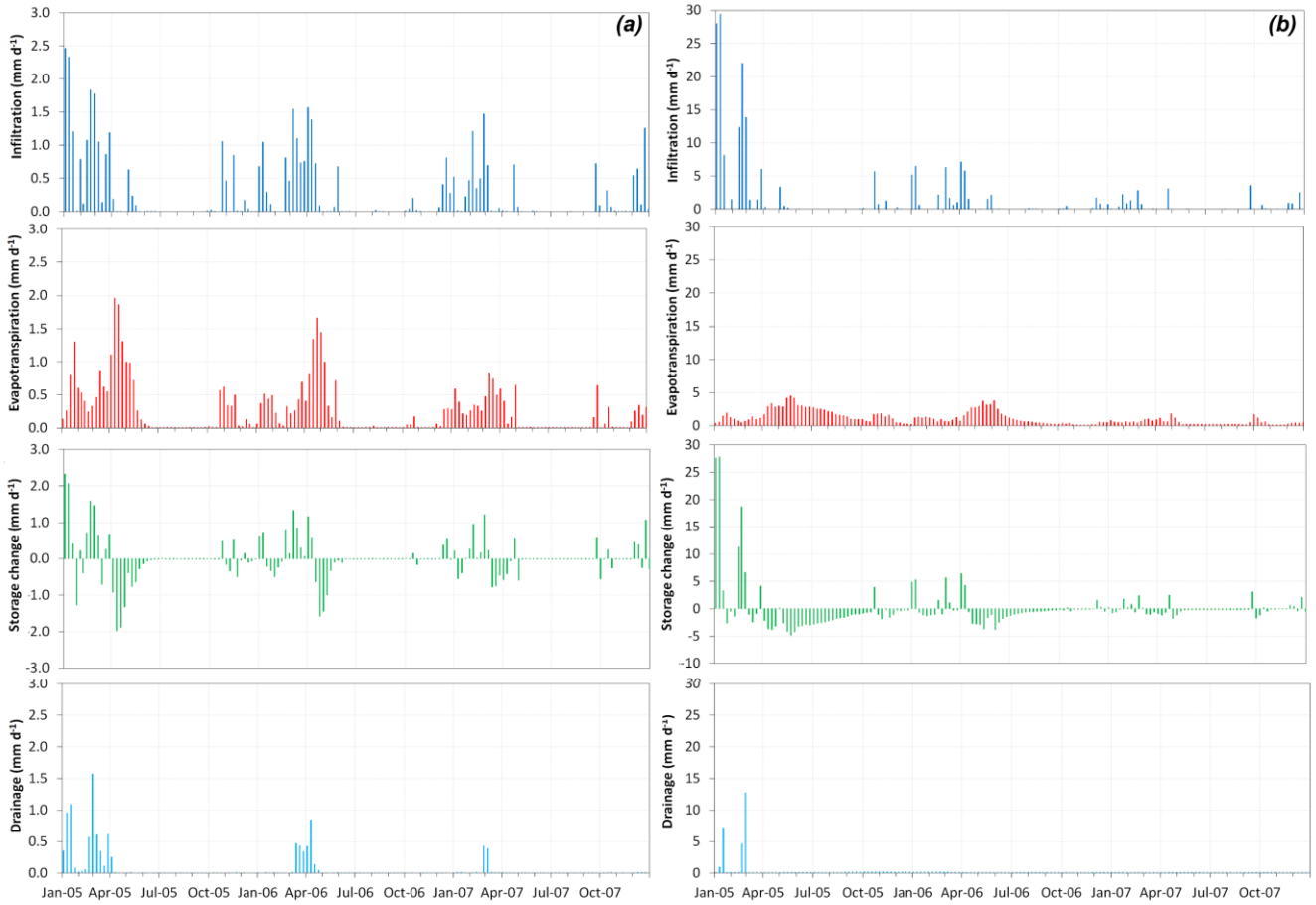

Figure 8 Unsaturated zone water budget for ET zone from January 2004 to December 2007 for two cells representative of the domain: (a) UZ-1 area with outcropping bedrock without vegetation; (b) UZ-2 area with alluvium deposit covered by vegetation.

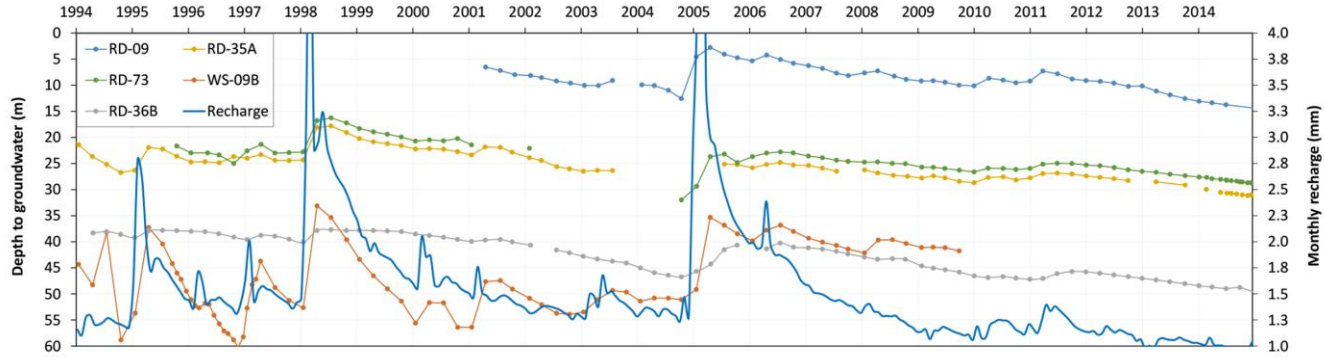

Figure 9 Comparison between the monthly recharge time series and the depth to groundwater at five locations across the catchment.

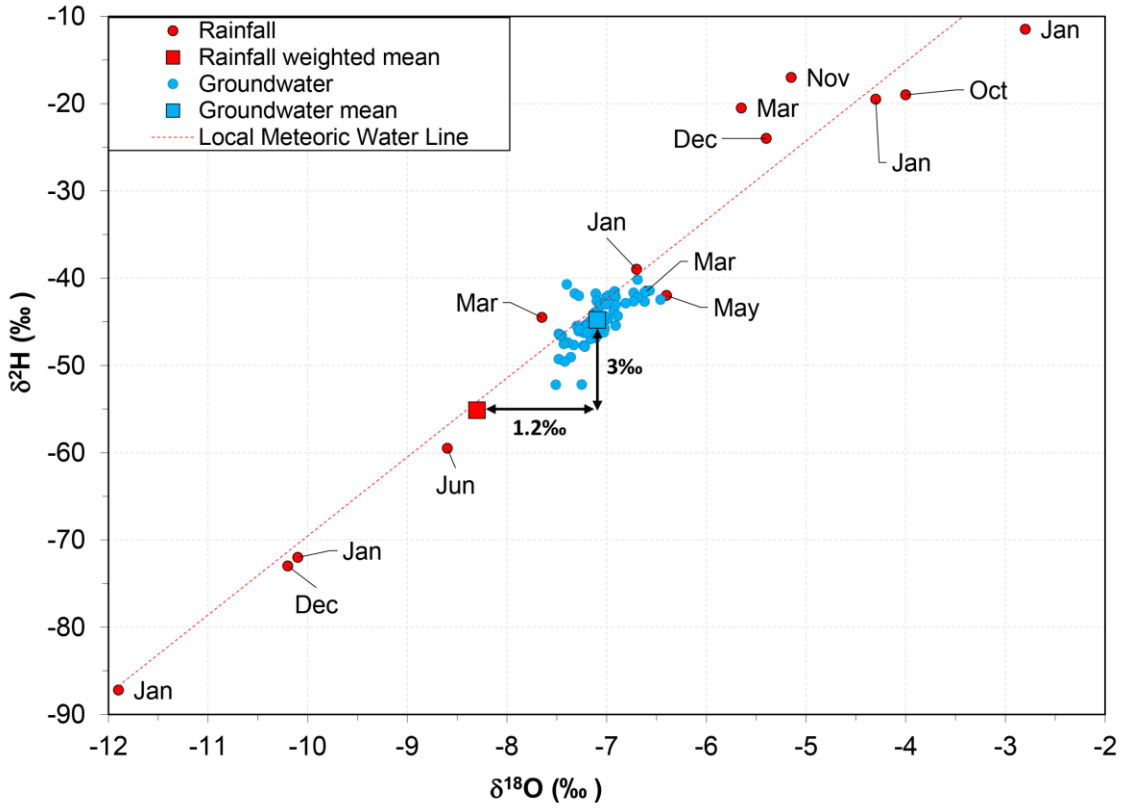

831

832 *Figure 10 Water isotopes plot for rainfall samples collected at two rain gauge stations and groundwater samples from 16*
833 *wells of the catchment.*

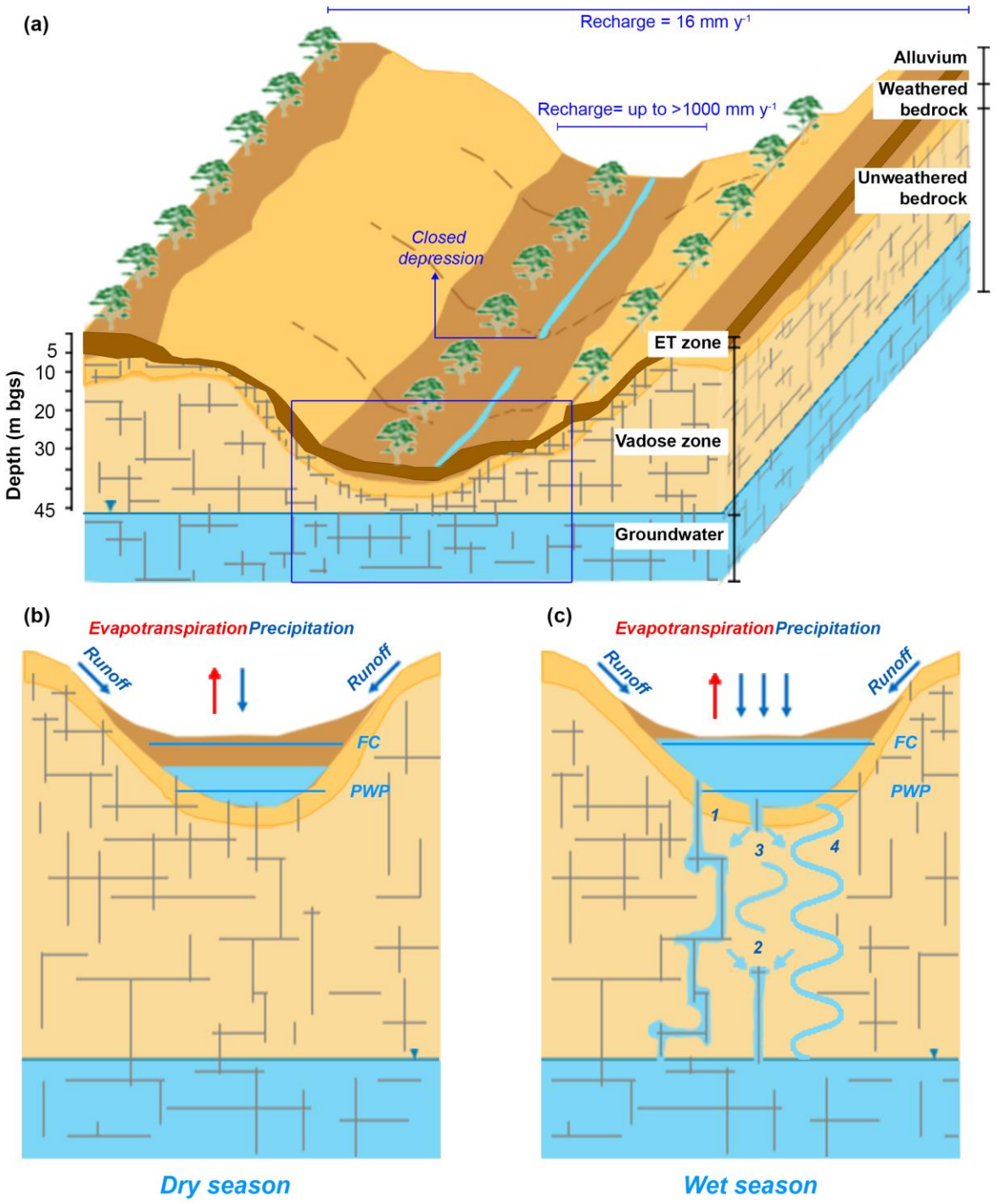

834

835 *Figure 11 Conceptual model for recharge at the site. (a) Spatial 3-D conceptual model of the catchment showing where high*
836 *recharge occurs. 2-D schematic of the unsaturated zone hydrologic process during (b) dry season and (c) wet season. During*
837 *the dry season water content is between the field capacity (FC) and the permanent wilting point (PWP) and therefore is*
838 *consumed by evapotranspiration. Conversely, during the wet season, water content is above the FC and seeps into the*
839 *underlying bedrock. Numbers describe mechanisms of flow in the vadose zone: 1 is fracture flow; 2 is water flowing from*
840 *matrix into fractures; 3 is water flux from fractures into matrix; 4 is intergranular matrix flow.*

841